Phonon-driven phase changes in $Cs_2LiCr(CN)_6$ †

R. R. Ryan
Los Alamos Scientific Laboratory, University of California, Los Alamos, New Mexico 87545

B. I. Swanson
Chemistry Department, University of Texas, Austin, Texas 78712

(Received 24 July 1975; revised manuscript received 8 January 1976)

Dicesium lithium chromicyanide $Cs_2LiCr(CN)_6$ undergoes first- and second-order phase changes at 348 and 310°K, respectively. The room-temperature structure is only slightly distorted from the high-temperature $Fm3m$ phase. While it was not possible to solve the room-temperature structure using diffraction methods alone, owing to complex multiple twinning, a suitable model could be found with the aid of light-scattering experiments and group theory. The first-order phase transformation at 348°K involves an antiferrodistortive rotation of the rigid $Cr(CN)_6^{3-}$ octahedron about the z axis of the cubic cell $\nu_{14}(X^{2+})$. The second-order instability at $T_c = 310$°K can be modeled as a soft cesium displacive mode at the X point $\nu_{16}(X^{5+})$. The room-temperature structure ($P2_1/n$) shows the largest distortions from the parent high-symmetry form only along these two phonon directions (6.2° rotation of the complex ion and a 0.09-Å translation of the Cs atom). The lattice instability in the $Cs_2LiCr(CN)_6$ crystal is attributable to a thermally excited Cs atom which occupies a site which is too large. Those $Cs_2LiM(CN)_6$ salts with smaller Cs holes ($M = Mn^{+3}$, Fe^{+3}, and Co^{+3}) exhibit $Fm3m$ cells at room temperature, supporting the suggestion that the size of the Cs environment determines the stability with respect to distortion along the $\nu_{14}(X^{2+})$ and $\nu_{16}(X^{5+})$ phonon directions.

INTRODUCTION

An increasing number of systems exhibiting structural phase changes have been studied over the past ten years. Much of the early work, which was stimulated to a large extent by Cochran[1-3] centered on ferroelectrics. There is, however, a growing literature concerning structural phase changes where both phases are paraelectric.[4,5] Perhaps the best studied structural type are the perovskites which exhibit both ferroelectric and antiferroelectric (or cell doubling) phase transitions. This report concerns the phase changes in a structurally related system, $Cs_2LiCr(CN)_6$.

The high-temperature phase of $Cs_2LiCr(CN)_6$ ($T > 348$ °K) is cubic $Fm3m$ while the high-symmetry phase of the perovskites is $Pm3m$. A major distinction between the perovskite structure and that of $Cs_2LiCr(CN)_6$ is the presence of the $Cr(CN)_6^{-3}$ complex ion whose internal forces are much stronger than the interionic potentials in the lattice. In perovskites such as $BaTiO_3$ there are no discreet complex ions with strong interatomic potentials, but rather a lattice of O atoms with Ti and Ba atoms occupying sites of O_h symmetry and Ti-O interaction strengths roughly on a par with Ba-O interactions. There are a vast number of crystalline systems which possess pseudorigid complex ions such as $Cs_2LiCr(CN)_6$, and these are of interest to the chemistry community from the standpoint of the interatomic forces in the complex ion itself. What is of immediate interest here is whether or not the structural phase changes in the crystalline systems containing rigid complex ions are tractable using the phonon language which has been so successful in describing the phase transitions in the simpler perovskites.

The $Cs_2LiCr(CN)_6$ salt is a member of the series $Cs_2LiM(CN)_6$ (M = Cr, Mn, Fe, Co, Ir) which has been probed in some detail using x-ray diffraction[6,7] and vibrational spectroscopic methods.[8-10] The principal goal of these early studies was to probe the internal forces of the complex ion as a function of the transition metal. In order to be able to attribute changes in the M-C and C-N bond lengths in the series to internal forces of the complex ion, it was essential that an isostructural series be studied, thereby eliminating any possible bond length variation resulting from changes in the packing forces. The dicesium lithium salts provided such an isostructural series. However, while Mn, Fe, and Co salts are $Fm3m$ at room temperature, the Cr and Ir salts are isostructural to the other members of the series only at elevated temperatures[7] ($T > 348$ and 418 °K, respectively).

While the high-temperature phase of the $Cs_2LiM(CN)_6$ salts are well characterized, the solution of the room temperature structure of $Cs_2LiCr(CN)_6$ proved to be an intractable problem using x-ray diffraction methods alone, even though the structural distortions were known to be slight on the basis of the low intensities of the non-$Fm3m$ reflections. It has been possible, however, to devise a structural model for the distorted phase using the x-ray observations, light scatter-

ing experiments and group theory. In the course of this report, we describe the dynamics of the complex phase changes and an evaluation of the room temperature static distortions in $Cs_2LiCr(CN)_6$.

CHARACTERIZATION OF THE PHASE CHANGES

The space group of the high-temperature phase (I) of $Cs_2LiCr(CN)_6$ is $Fm3m$ with a cell constant of 10.780 Å at 381 °K. The $Cr(CN)_6$ moiety occupies position $4a$ (O_h symmetry), the lithium atom $4b$ (O_h), and the Cs atom $8c$ (T_d). The structure of this phase was determined by conventional single-crystal x-ray techniques.[7] We have established the existence of two phase changes between this phase and room temperature using x-ray, Raman, optical, and ^{133}Cs NMR methods.

The first of these (to phase II) occurs at 348° ± 3 °K and is characterized by the appearance of a broad, weak feature at approximately 100 cm^{-1} in the Raman spectrum which splits into two components at low temperature (~ 98 and 112 cm^{-1}, Fig. 1). In addition, the optical properties exhibit a sharp isotropic-anisotropic transition at this temperature. X-ray measurements taken at 326 °K indicate this phase to be tetragonal with cell constants $a = 7.604(2)$ and $c = 10.777(3)$ Å. The temperature dependence of the reflection (320) with the highest intensity (of the general class which are characteristic of the tetragonal cell) is shown in Fig. 2. This phase change has been further corroborated by ^{133}Cs NMR measurements[11] which exhibit hysteresis over the range 344–354 °K (scan rate 5° per hour). Although

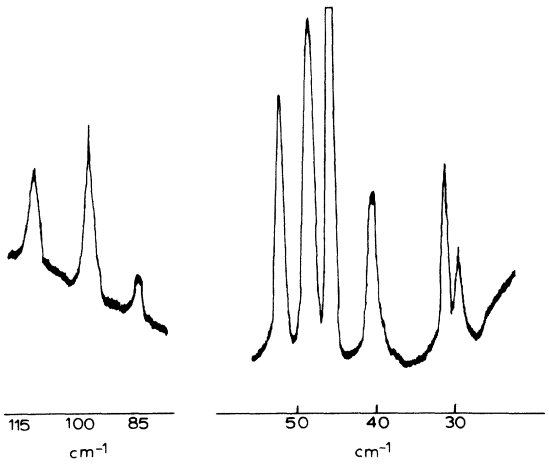

FIG. 1. Raman spectrum of $Cs_2LiCr(CN)_6$ below 120 cm^{-1} at 20 °K.

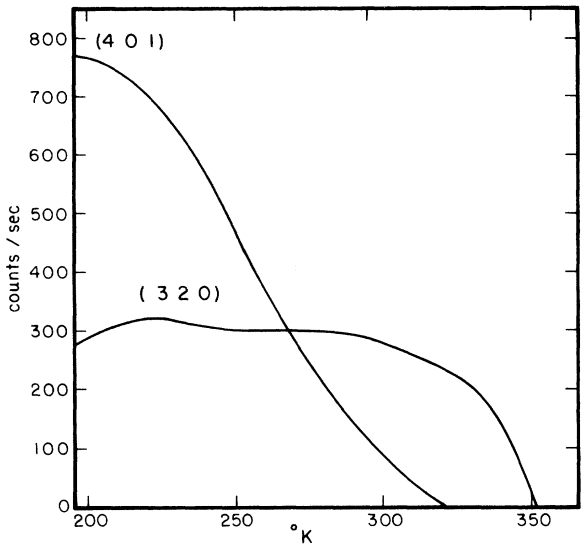

FIG. 2. Plot of the intensity of (401) and (320) as a function of temperature.

the temperature dependence of the (320) reflection does not show a sharp discontinuity, the hysteresis in the NMR measurements and the absence of a Raman-active vibration, whose frequency tends to zero at the transition temperature, suggests this phase change to be first order.

As the crystal is cooled below room temperature, several new features emerge in the Raman spectrum. The region below 50 cm^{-1}, where ν_{17} is the only mode observed in the $Fm3m$ phase, is shown in Fig. 3. The most striking feature is a new mode which emerges from the Rayleigh line, hardening to ~31 cm^{-1} at 20 °K. A plot of the square of the frequency for this mode as a function of temperature (Fig. 4) shows the linear dependence characteristic of a second-order phase change. The critical temperature obtained by extrapolating the square of the soft mode frequency to zero is 310 °K, some 40° *below* the temperature at which the crystal becomes isotropic. This large disparity cannot be accounted for on the basis of local heating; we estimate the errors for the temperature in this Raman experiment to be no more than ± 5°. The above implies that there are two phase changes occurring; a first-order change at 348 °K where the crystal becomes isotropic, and a second-order phase change at 310 °K (to phase III). The existence of the second phase change is further evidenced by the appearance of a new class of reflections in the x-ray pattern, with indices of the type hOl, $l = 2n+1, h = 2n$, whose intensities also increase in a manner characteristic of a second-order transition as the temperature is lowered. The strongest of

these may be indexed as (401) on the tetragonal cell and is plotted in Fig. 2. The phase change as determined from this plot appears to be 317 °K.

The exact nature of the structural changes involved in these two phase transformations are, in principle, most conveniently elucidated by the straightforward application of conventional single-crystal x-ray techniques. However, two observations indicate that the solution to the structure of this material would be extremely difficult, if not impossible, using conventional techniques. First, the optical properties of the crystals show evidence for complicated multiple twinning. Second, the set of reflections which can be indexed on the higher symmetry $Fm3m$ cell are extremely strong relative to the rest of the diffraction pattern. A refinement of the structure in the $Fm3m$ space group results in a crystallographic R value

$$R = \sum (|F_0'| - |F_c'|)/\sum |F_0'|$$

of 2.5% indicating the true structure to be only a slight distortion from the $Fm3m$ structure. This latter point and the observation that one of the low-lying vibrational frequencies is soft, point to the possibility that the distortion can be described in terms of the phonon language developed for second-order phase transitions.[1-3,12,13] We outline the important Raman and x-ray results in the following paragraphs. A more complete description of these results and of the notation appearing in the figures, tables, and text will be found in the appendix.

The room temperature diffraction pattern (phase III) shows Laue symmetry $4/mmm$ and is indexable on the same primitive cell as is phase II. The extinction conditions are: Okl (hOl), $l = 2n$ when $k(h) = 2n + 1$ and (OOl), $l = 2n + 1$. Note that the first extinction condition is not required by any space-group symmetry operator. This observation subsequently proved to be invaluable in identifying the lower-temperature phase change. The lower symmetry cells are twice the volume of the primitive cell of the $Fm3m$ structure and the relationship between them establishes that the structural distortion in phase II is described in terms of an X point phonon in phase I. Similarly, phase III is related to phase II by a phase II Γ point phonon. It is important to notice that the Γ point phonon of phase II is in turn describable as an X point vibration of phase I, i.e., all phase I Γ point phonons produce body centered cells and are incapable of giving rise to the set of reflections unique to phase III. In order to derive the space group for the room-temperature phase it is therefore sufficient that it be subduced[14] by the representations for two phase I X-point phonons *simultaneously*.

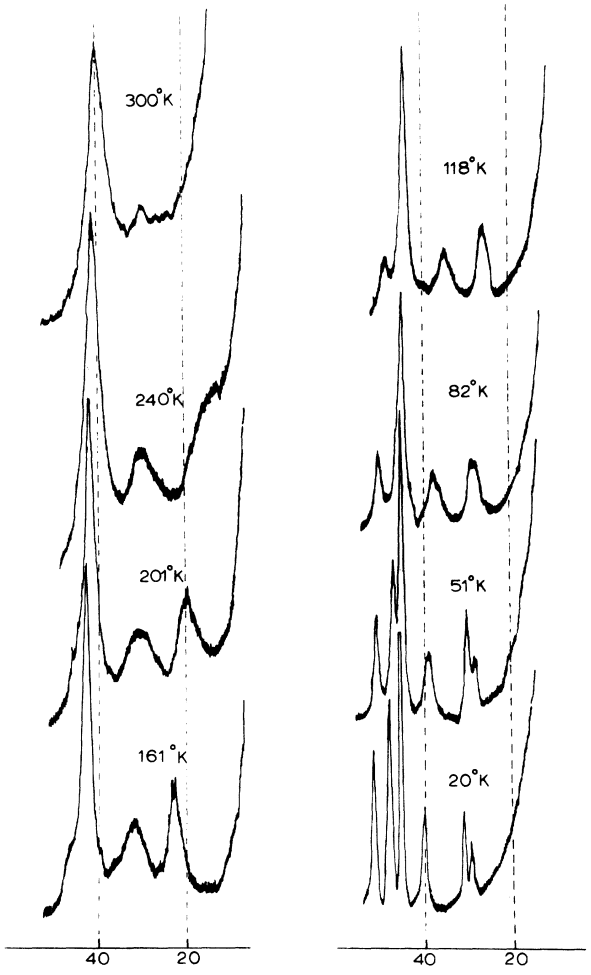

FIG. 3. Raman spectra of the low-energy region of $Cs_2LiCr(CN)_6$ as a function of temperature.

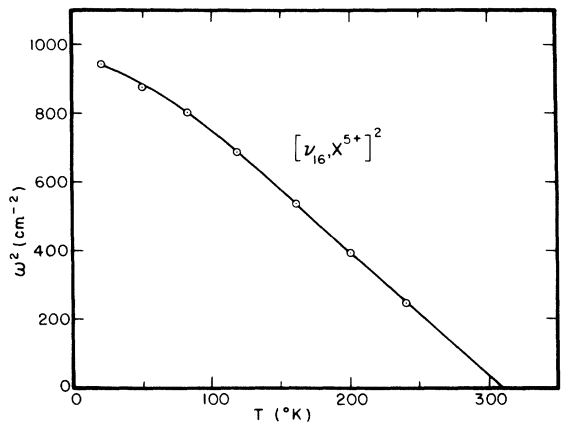

FIG. 4. Square of the frequency of X^{5+} vs temperature.

The $Cr(CN)_6^{-3}$ internal modes do not change greatly upon cooling the crystal from the high-temperature $Fm3m$ phase to the distorted phase at ~20 °K, except for splittings observed at the lower temperatures (see below). The implication here is that the phase change does not involve a significant distortion of the $Cr(CN)_6^{-3}$ octahedron. This greatly simplifies the problem since we need consider only external modes in defining the phase change: the distortion may, however, involve translation or rotation of the rigid octahedron.

The Raman observations were also useful in characterizing the soft mode associated with the second-order phase change at 348 °K. From consideration of the frequency of the soft mode and the splitting patterns for internal and external phonons at 20 °K, the soft mode could be assigned to the doubly degenerate Cs displacive mode (X_a^{5+}) whose progenitor is the F_{1u} Cs translation in phase I (ν_{16}, Γ^{4-}). As explained in the Appendix, convincing arguments based on all of the physical measurements can be made for a structural model in which the phase-I to phase-II transition is describable in terms of an antiferrodisplacive rotation of the octahedron (X^{2+}) resulting in the space group $P4/mnc$. These distortions are depicted in Fig. 5. The space group generated by distortions of the parent high symmetry $Fm3m$ cell is $P2_1/n$. The tetragonal diffraction observed for $Cs_2LiCr(CN)_6$ at room temperature results from a 50-50 twin of the $P2_1/n$ cell across the (110) plane. The magnitude of the coefficients of the symmetry coordinates describing the structural distortions have been determined by least-squares refinement of this model to the room temperature x-ray intensities, in the space group $P2_1/n$.

The principal distortions (from the parent $Fm3m$ cell) in the refined structure can be described in terms of the two phonons used to derive the space group ($P2_1/n$), i.e., a Cs displacement of 0.09 Å in the y direction corresponding to the X_a^{5+} phonon and a rotation of the octahedron of 6.5° about z corresponding to the X^{2+} phonon. Rotations of the octahedron about the x direction also transform as X_a^{5+} and this parameter, which is denoted by Θ_x in Table V, refines to a value of $-0.1(1)°$. The space group $P2_1/n$ allows two additional degrees of freedom for the Cs atom (x and z) and one for rotation of the octahedron (Θ_y) which correspond to Γ point vibrations in the $Fm3m$ cell. The full matrix refinement produces values for these parameters which are extremely close to those exhibited by the $Fm3m$ structure. The validity of the model for the phase changes presented here is strongly supported by its agreement with all of the physical measurements and the observations that all structural and thermal parameters are physically reasonable.

DISCUSSION

The lattice instability in $Cs_2LiCr(CN)_6$ is similar in nature to the cell doubling transitions in perovskites.[5] The R point transitions in $MTiO_3$ (M = Ba, Sr, etc.) can be simulated as rotations of the TiO_6 framework with respect to the counter ion. In $Cs_2LiCr(CN)_6$, a antiferrodistortive rotation occurs followed by a translation of the Cs atoms.

For the $Cs_2LiM(CN)_6$ salts there appears to be a direct connection between the size of the Cs site and the lattice instabilities. In proceeding from Cr through Co the lattice shrinks monotonically [a = 10.780(2) and 10.495(1) Å for Cr and Co, respectively], thereby reducing the size of the Cs site. The closest atom to Cs is N and the Cs-N distance decreases from 3.842(1) Å in $Cs_2LiCr(CN)_6$ to 3.733(1) Å in the Co salt.[6,7] The reduction in the Cs hole size is accompanied by reductions in the Cs, C, and N thermal motions.

The unusually large Cs-N distance (~0.5 Å larger than that predicted from ionic radii) and the abnormally high Cs thermal motion, are consistant with the observation that the lattice instability in $Cs_2LiCr(CN)_6$ involves a soft Cs displacive mode. Furthermore, the $Cr(CN)_6^{-3}$ rotation can be attributed to the same origin since this mode can be described in terms of Cs-CN coordinates in the harmonic approximation.[8] The picture which now emerges is that as the Cs hole size is increased in going from Co → Cr the cubic lattice becomes unstable with respect to distortion. This may ex-

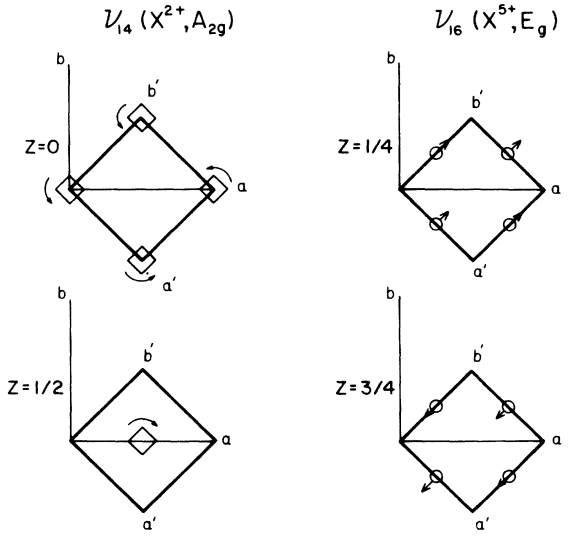

FIG. 5. Schematic of the observed distortions.

plain why the Mn, Fe, and Co salts are all $Fm3m$ at room temperature while the Cr salt is not. We might anticipate that the Ir salt, whose lattice size [10.720(3) Å] is close to that of the Cr salt, might also exhibit a similar instability above room temperature. This expected instability has been verified by light scattering studies.[15]

The $Cs_2LiM(CN)_6$ series brings up interesting possibilities as regards the connection between ion sizes, site sizes, and lattice instabilities. Correlations of ion sizes with lattice instabilities have been made for the rare-earth aluminates $MAlO_3$ (M = La, Pr, Nd, Sm) where a decrease in the size of the rare-earth ion raises the observed transition temperature. That is, a large rare-earth ion more effectively stabilizes the cubic lattice driving the transition temperature down.[16] Similar correlations have been made for the perovskites $MTiO_3$ (M = Sr, Ba, Pb). However, the trends are somewhat complicated in this latter series by obvious changes in interionic potentials and mass effects.

The intriguing aspect of the $Cs_2LiM(CN)_6$ salts is that one can systematically effect a change in the Cs hole size by varying transition metal without dramatically changing the interionic potentials (the Li-N and Cs-CN interactions) or the mass of the complex ion. In this case one might be able to correlate a site size with lattice instabilities. Work is now underway to fully characterize the phase changes in the $Cs_2LiM(CN)_6$ salts.

The authors are indebted to Dr. Eiichi Fukushima for the NMR measurements, and to Dr. Allen C. Larsen for writing the L.S. code for twinned crystals. We are also indebted to Dr. John L. Warren, Dr. John Axe (Brookhaven National Laboratory), and to Dr. Eiichi Fukushima for helpful discussions, and to Bonnie Lucas for help in collecting some of the x-ray data.

APPENDIX A: SPECTROSCOPY

The selection rules, vibrational spectra, and assignments for the cubic $Fm3m$ phase of $Cs_2LiCr(CN)_6$ have already been discussed.[9] Since the $Cr(CN)_6^{-3}$ moiety occupies a site of O_h symmetry and only one molecule need be considered in the factor group, the selection rules for the hexacyanide group internal modes do not change in going from the isolated ion to the $Fm3m$ lattice. In addition to the internal modes there is one inactive rotatory mode (ν_{14}, F_{1g}) and three translatory modes (ν_{15} and ν_{16}, F_{1u} infrared active and ν_{17}, F_{2g} Raman active). An approximate description of the observed fundamentals and their corresponding frequencies are given in Table I.

Raman spectra were observed as a function of temperature using a Cary 82 spectrometer and an Air Products closed-cycle He cryostat (Displex). A single crystal of $Cs_2LiCr(CN)_6$ was coupled to the copper cold finger using Crycon grease and the temperature was monitored using a thermocouple which was also coupled to the

TABLE I. Zone center assignments for $Cs_2LiCr(CN)_6$ (cm^{-1} at 298 °K) and zone-boundary selection rules.

Description	Zone center	Frequency	Zone boundary (D_{4h})
ν_1 (CN Stretch)	A_{1g} (Γ^{1+}, R)	2139.8	$A_{1g}(X^{1+})$
ν_3 (CN Stretch)	E_g (Γ^{3+}, R)	2141.3	$A_{1g}(X^{1+}) + B_{1g}(X^{3+})$
ν_6 (CN Stretch)	F_{1u} (Γ^{4-}, ir)	2138.5	$A_{2u}(X^{2-}) + E_u(X^{5-})$
ν_7 (CrCNδ)	F_{1u} (Γ^{4-}, ir)	468.5	$A_{2u}(X^{2-}) + E_u(X^{5-})$
ν_{10} (CrCNδ)	F_{2g} (Γ^{5+}, R)	385	$B_{2g}(X^{4+}) + E_g(X^{5+})$
ν_2 (CoC Stretch)	A_{1g} (Γ^{1+}, R)	381.5	$A_{1g}(X^{1+})$
ν_4 (CrC Stretch)	E_g (Γ^{3+}, R)	381.5	$A_{1g}(X^{1+}) + B_{1g}(X^{3+})$
ν_8 (CrC Stretch)	F_{1u} (Γ^{4-}, ir)	360.7	$A_{2u}(X^{2-}) + E_u(X^{5-})$
ν_{15} (Li lattice mode)	F_{1u} (Γ^{4-}, ir)	300	$A_{2u}(X^{2-}) + E_u(X^{5-})$
ν_{11} (CCrCδ)	F_{2g} (Γ^{5+}, R)	175.7	$B_{2g}(X^{4+}) + E_g(X^{5+})$
ν_9 (CCrCδ)	F_{1u} (Γ^{4-}, ir)	164.0	$A_{2u}(X^{2-}) + E_u(X^{5-})$
ν_{14} (rotatory)	F_{1g} (Γ^{4+}, silent)	...	$A_{2g}(X^{2+}) + E_g(X^{5+})$
ν_{16} (Cs lattice mode)	F_{1u} (Γ^{4-}, ir)	56.5	$A_{1g}(X^{1+}) + E_g(X^{5+})$
ν_{17} (Cs lattice mode)	F_{2g} (Γ^{5+}, R)	40.9	$B_{1u}(X^{3-}) + E_u(X^{5-})$

copper block. Raman spectra were obtained using ~100 mW of the red line of a Spectra Physics 164 Kr^+ laser (6471 Å). Spectra above room temperature were obtained by controlled heating of a single crystal mounted on a fiber in a dry N_2 stream.

As shown in the text, the phase change involves X-point modes. Thus, we will only consider the symmetry coordinates for the Γ and X-point lattice modes. The rotatory mode ν_{14} at $k=0$ (k being the phonon wave vector) involves an in-phase rotation of the $Cr(CN)_6^{-3}$ octahedron. For the F_{1u} Cs lattice mode all the Cs atoms move in the same direction, while for the F_{2g} symmetry mode the two Cs atoms in the primitive cell move out of phase with respect to one another. At the X point all of the triply degenerate modes branch into two components each, one of which is doubly degenerate. The symmetries for the various X-point modes are given in Table I. For simplicity in presentation, we have considered only Cs atom movement for the F_{1u} lattice mode ν_{16}. Spectra at room temperature show weak features at ~30 and 100 cm^{-1} which are not observed for the other $Cs_2LiM(CN)_6$ salts known to be cubic $Fm3m$. When $Cs_2LiCr(CN)_6$ is heated beyond the phase change at 348 °K, these two features disappear and the resulting spectra appear identical to those of the other $Fm3m$ salts. It should be noted that the intensity of the F_{2g} Cs mode, ν_{17}, increases relative to the F_{2g} CCrC deformation mode ν_{11} as the crystal is heated.

Several new features emerge in the low-energy region as the crystal is cooled below room temperature (Fig. 3). The most notable new band is the soft mode which hardens to 31 cm^- at 20 °K. The square of the frequency of this mode varies linearly with temperature, as is typical of a second-order phase change (Fig. 4).

The band observed at 30 cm^{-1} at room temperature hardens to 41 cm^{-1} at 20 °K. The broad weak feature at ~ 100 cm^{-1} in the room temperature spectrum splits into two components at low temperature (98 and 112 cm^{-1}) and a new band is observed at 85 cm^{-1} (Fig. 1). The frequency dependence of the low-energy modes as a function of temperature is shown in Fig. 6. At this point tentative assignments of the new low-temperature bands were made on the basis of their observed frequencies and splitting patterns. The reasoning is as follows: Swanson and Jones[8] carried out a normal mode of calculation for the isotypic salt $Cs_2LiCo(CN)_6$ ($Fm3m$ phase) where interionic potentials were included. Using the potential function obtained for $Cs_2LiCo(CN)_6$ the $Co(CN)_6^{-3}$ rotatory mode was estimated to be ~ 100 cm^{-1}. Thus, the three features at 85, 98, and 112 cm^{-1}

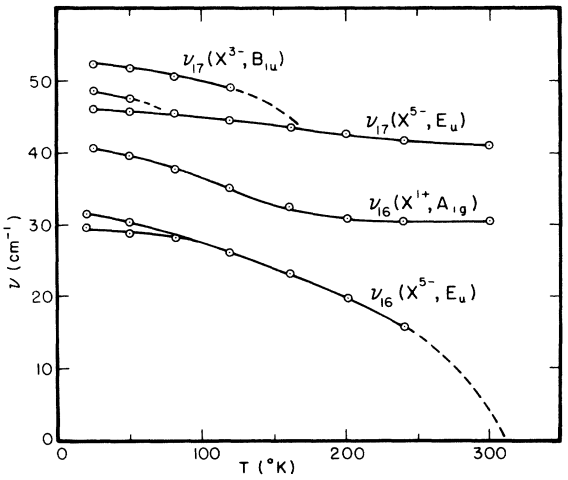

FIG. 6. Frequency response of the translatory lattice modes of $Cs_2LiCr(CN)_6$ as a function of temperature.

have been attributed to $Cr(CN)_6^{-3}$ rotatory modes made active by the phase change. The soft mode and the new feature at 41 cm^{-1} were then attributed to Cs translatory modes; this latter assignment is reasonable since the $Fm3m$ active Cs modes, ν_{16} and ν_{17}, were both observed below 60 cm^{-1} in the cubic phase. It should be noted that the five new features discussed above cannot be attributed to internal modes as they are too low in energy.

Although the doubling of the volume of the primitive unit cell allows the possibility of factor group splittings, the splitting patterns (Fig. 7) indicate that these are small enough to be neglected. The lower site symmetry which removes the degeneracy of the cubic phase modes is readily apparent at low temperature for the internal vibrations. In general, doubly degenerate modes are observed to split into two components while triply degenerate modes give three new bands. Similarly, only three components are observed for the rotatory mode, instead of the six to be expected if correlation group splitting were important.

The F_{2g} Cs lattice mode remains as a single band until low temperature where it splits into three components. The similarity between the internal modes and the F_{2g} Cs lattice mode, insofar as the temperature dependence of the splitting is concerned, suggests that the three bands at 52, 49, and 47 cm^{-1} emanate from the F_{2g} Cs lattice mode. Thus, the soft mode can only be attributed to the F_{1u} Cs lattice mode. Also, since the soft mode is observed to split at extremely low temperatures, we can assign it to the doubly degenerate component of the $F_{1u}(\Gamma)$ Cs mode. This assignment indicates that the second-order

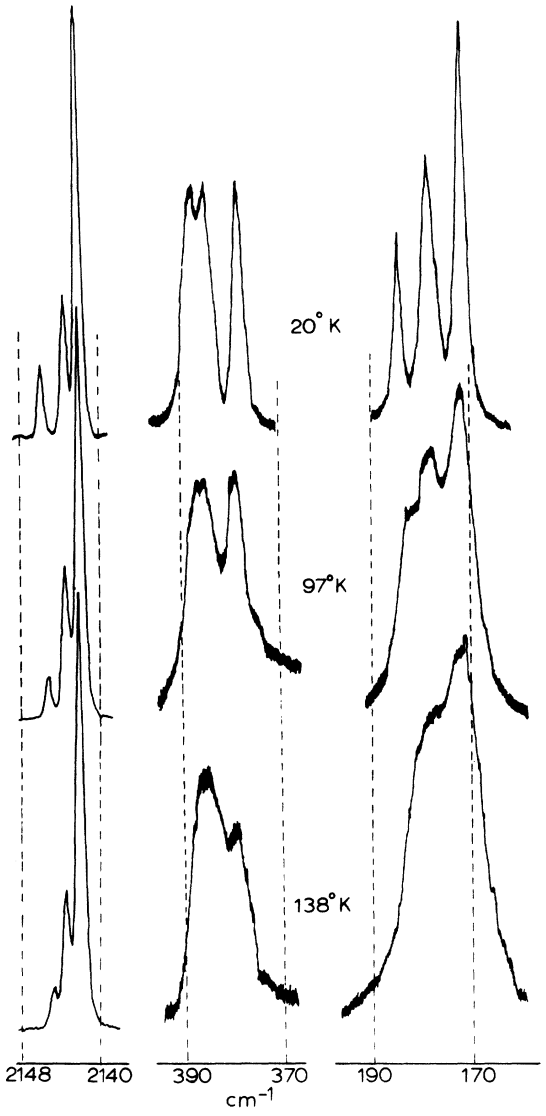

FIG. 7. Raman spectra of the internal modes of $Cs_2LiCr(CN)_6$ at low temperature.

phase change observed at 310 °K is driven by $E_g(X^{5+}, Cs)$ (see Fig. 5).

An alternative explanation for the features at 52 and 41 cm^{-1} (20 °K) would be to reverse their assignments. Thus, the 52 cm^{-1} band, which appears only at low temperature, is assigned to the nondegenerate component of the F_{1u} Cs mode (X^{1+}, Cs) while the lower-energy mode is attributed to the nondegenerate component of the F_{2g} Cs mode (X^{3-}, Cs). These latter assignments are consistent with the observation that the 52 cm^{-1} band appears to grow in intensity, rather than to split off from the F_{2g} Cs mode (see Fig. 3). Definitive assignments of these two bands must await a more detailed investigation of the spectrum

TABLE II. Observed Raman modes (cm^{-1}) for the distorted phase of $Cs_2LiCr(CN)_6$ at 20 °K.

$\nu_1(X^{1+})$ [a]	2142.5
$\nu_2(X^{1+})$	378.6
$\nu_3(X^{1+}$ and $X^{3+})$	2146.3, 2144.0
$\nu_4(X^{1+}$ and $X^{3+})$	...
$\nu_{10}(X^{4+}$ and $X^{5+})$	388.0, 385.4
$\nu_{11}(X^{4+}$ and $X^{5+})$	184.4, 178.7, 172.0
$\nu_{14}(X^{2+}$ and $X^{5+})$	111.8, 97.9, 81.4
$\nu_{16}(X^{1+})$ or $\nu_{17}(X^{3-})$	40.8
$\nu_{16}(X^{5+}$, soft mode)	31.6, 30.0
$\nu_{17}(X^{3-})$ or $\nu_{16}(X^{1+})$	52.5
$\nu_{17}(X^{5-})$	48.7, 46.1

[a] See Table I for an approximate description of the observed modes.

of phase II (X^{3-} is Raman-active in phase II while X^{1+} is not). It should be noted that the ambiguity in assignment of the 52 and 41 cm^{-1} features does not alter our conclusions as regards the assignment of the soft mode. The observed frequencies and their assignments for the low-temperature phase at 20 °K are given in Table II.

APPENDIX B: SPACE-GROUP CONSIDERATIONS

The techniques for the derivation of the lower symmetry space groups are well known and involve finding a space group (G') for which the density function $\rho(\mathbf{r}) = \rho_0(\mathbf{r}) + \delta\rho(\mathbf{r})$ is invariant; $\rho_0(\mathbf{r})$ is the density function of the higher symmetry space group (G) and $\delta\rho(\mathbf{r})$ is the expansion in terms of the irreducible representations for G', i.e., $\sum_{ij} C_{ij}\phi_{ij}(\mathbf{r})$ where the ϕ_{ij}'s form the j-dimensional bases for ith irreducible representation. With the aid of the proper symmetry tables[17,18] all of the space groups which are consistent with the X-point phonons in the $Fm3m$ cell can be generated (Table III).

The space groups resulting from consideration of the X-point phonons taken two at a time are easily derived by requiring that the density function $\rho(\mathbf{r}) = \rho_0(\mathbf{r}) + \rho^1(\mathbf{r}) + \rho^2(\mathbf{r})$ remain invariant with respect to all operations, where $\rho^1(\mathbf{r})$ and $\rho^2(\mathbf{r})$ are invariant under operations of the space

TABLE III. Space groups produced by the X-point lattice phonons. x and y refer to the primitive tetragonal coordinate system.

No.	Phonon label	Space group	Phonon
1	X^{1+}	D_{4h}^{1} ($P4/mmm$)	Cs in phase z motion [a]
2	X^{2+}	D_{4h}^{6} ($P4/mnc$)	Rotation about z axis
3	X^{2-}	D_{4h}^{7} ($P4/nmm$)	Li, octahedron z motion
4	X_a^{5+}	D_{2h}^{12} ($Pnmn$)	Cs in phase $x+y$ motion } octahedron
5	X_b^{5+}	D_{2h}^{18} ($Ccma$)	Cs in phase x motion } rotation
6	X_a^{5-}	D_{2h}^{13} ($Pnmm$)	Li, Cs out of phase $x+y$ motion } octahedron
7	X_b^{5-}	D_{2h}^{17} ($Cmnm$)	Li, Cs out of phase x motion } translation
8	X^{3-}	D_{4h}^{15} ($P4_2/nmc$)	Cs out of phase z motion

[a] "in phase" refers to the two Cs atoms in the primitive F_{m3m} cell.

group they generate individually. As one would expect, since two phase changes have taken place, the room-temperature single-crystal diffraction pattern is not explicable in any of the one phonon space groups even when the effects produced by a twinned crystal are taken into account. However, the Raman spectra strongly suggest that the phase-I to phase-II transition is related to X^{2+} and that the lower-temperature transition is describable in terms of X^{5+}. Of the two X^{5+} orthorhombic space groups, $Ccma$ (X_b^{5+}) may be rejected because it produces reflections which are not observed, i.e., it violates the (Okl) extinction condition. On the other hand, neither $Pnmn$ (X_a^{5+}) nor $P4/mnc$ (X^{2+}) produce reflections which violate the observed extinctions. Although it would appear that the mirror plane perpendicular to the b axis in $Pnmn$ is inconsistent with the (Okl) condition a simple calculation shows the distortion described by the X_a^{5+} symmetry coordinate produces the required diffraction pattern. The space group whose totally symmetric representation is subduced by the irreducible representation of X_a^{5+} and X^{2+} (simultaneously) is $P2_1/n$ where the 2_1 axis is a in the tetragonal cell. The calculated pattern which results from consideration of a 50-50 twin of $P2_1/n$ in which the twin relationship is a mirror plane containing the c axis and reflects the ac plane into the bc plane produces a diffraction pattern which is entirely consistent with the observed pattern. All other space groups produced by combination of the X point external symmetry coordinates can be rejected on the basis of considerations similar to those applied to $Ccma$.

APPENDIX C: X-RAY MEASUREMENTS AND REFINEMENT

A small twinned crystal whose largest dimension was 0.2 mm and which exhibited well-developed faces was selected and mounted on a fiber parallel to the c axis and used in all subsequent measure-

TABLE IV. Fractional coordinates and mean-squared amplitudes for the constrained least-squares calculations.

Atom	x [c]	y [c]	z [c]	μ_{11}	μ_{22}	μ_{33}	μ_{12}	μ_{13}	μ_{23}
Cs	0.500(2)	0.0085(1)	0.2501(5)	0.064(2)	0.057(2)	0.050(1)	−0.164(4)	−0.009(7)	−0.005(7)
Cr	0	0	0	0.017(2)	0.030(3)	0.020(1)	0.001(1)	−0.005(1)	−0.001(1)
Li	0	0	$\frac{1}{2}$	0.039(5)					
C_1	0.1685	0.2102	0.0024	0.036(1) [a]					
C_2	−0.2102	0.1685	−0.0019	0.036(1) [a]					
C_3	−0.0043	−0.0009	−0.1905	0.036(1) [a]					
N_1	0.2617	0.3265	0.0038	0.064(1) [b]					
N_2	0.3265	0.2617	−0.0030	0.064(1) [b]					
N_3	−0.0067	−0.0015	0.2959	0.064(1) [b]					

[a] Constrained to be equal.

[b] Constrained to be equal.

[c] For the carbon and nitrogen atoms (x, y, z) are calculated from the refined rotations of the octahedron and the refined average values for the Cr-C distance 2.053(5) Å, and the Cr-N distance, 3.190(6) Å. Rotations are defined by the rotation matrices $(R\theta_x)R(\theta_y)R(\theta_z)$, where $\theta_x = -0.1(1)°$, $\theta_y = +0.9(1)°$, and $\theta_z = -6.3(1)°$ about a, b, and c.

TABLE V. Fractional coordinates and mean-squared amplitudes for the unconstrained least-squares refinement.

Atom	x	y	z	μ_{11}	μ_{22}	μ_{33}	μ_{12}	μ_{13}	μ_{23}
Cs	0.5000(2)	0.0085(1)	0.2501(5)	0.064(2)	0.057(2)	0.050(1)	−0.0164(4)	−0.0009(7)	−0.0005(7)
Cr	0	0	0	0.017(2)	0.030(3)	0.020(1)	0.0011(1)	−0.0045(1)	−0.0006(1)
Li	0	0	$\frac{1}{2}$	μ =	0.039				
C_1	0.175(1)	0.207(1)	−0.002(1)	0.028(4)	0.056(6)	0.047(6)	−0.0005(4)	−0.014(4)	0.025(4)
C_2	−0.212(1)	0.163(1)	−0.004(1)	0.016(3)	0.034(4)	0.046(6)	0.005(3)	0.0006(4)	0.008(4)
C_3	−0.003(1)	0.000(1)	−0.1905(5)	0.063(4)	0.036(8)	0.024(3)	−0.007(5)	−0.0002(5)	−0.0023(4)
N_1	0.264(1)	0.330(1)	0.000(1)	0.022(3)	0.062(5)	0.074(6)	−0.018(3)	0.003(5)	0.007(5)
N_2	−0.325(1)	0.265(2)	−0.001(1)	0.033(5)	0.0108(8)	0.039(5)	−0.0141(12)	0.004(8)	0.015(7)
N_3	−0.004(1)	−0.004(1)	0.2977(5)	0.092(17)	0.085(15)	0.021(3)	−0.016(8)	0.013(6)	0.003(5)

ments. The cell constants were determined by least-squares refinement to 12 high-order reflections whose setting angles were measured on a Picker FACS-I system equipped with a graphite monochromator using the Mo $K\alpha$ line ($\lambda = 0.7093$ Å). The cell constants so determined are $a' = b' = 7.600(2)$, $c' = 10.778(3)$ Å. The cell angles were all 90° within the experimental error. Omega scans of several reflections showed a half-width at half-height of less than 0.2° and no evidence of splitting due to the twinning.

Intensities were measured using 2° Θ-2Θ scans at a scan rate of 1°/min for an octant of data ($h, k, l \geq 0$) to a maximum 2Θ value of 70°. The intensities were corrected for the usual Lorentz and polarization factors and for absorption. "Equivalent" reflections, assuming $4/mmm$ symmetry, when averaged, gave an agreement index of less than 2% for all classes of reflections. The averaged data were used in the refinement of the structure.

The model for the structure in $P2_1/n$ requires the Cr atom of the octahedron to occupy the $\bar{1}$ site at 000 (2a), the lithium atom in 2b at $00\frac{1}{2}$ and the Cs atom in the general position 4c with the approximate coordinates $\frac{1}{2}$, Δy, $\frac{1}{4}$, where Δy is a small displacement of the Cs y coordinate from $y = 0$ caused by the X^{5+} phonon. The $Cr(CN)_6$ moiety was assumed, on the basis of the spectroscopic measurements, to maintain octahedral symmetry and was refined as a rigid body, the adjustable parameters being rotations about the z axis corresponding to X^{2+}, about the x axis (X^{5+}) and about y (Γ^{4+}). In addition, two parameters describing the totally symmetric (in O_h) "breathing" motions of the octahedron were allowed to vary which, in effect, allowed the refinement of the average Cr-C and C-N distances.[19] All carbon atoms were constrained to have equal isotropic thermal parameters as were the nitrogen atoms. Notice that the placement of the Cs atoms in a general position allows degrees of freedom in the x and z directions which can be described in terms of a Γ point translational motion in addition to the X-point y displacement.

Except for the modifications necessary to describe the intensities in terms of the proposed twinning mechanism, the least-squares refinement was carried out as in previous work.[7] The function minimized was $\sum \omega_i (I_i^0 - I_i^c)^2$ where $\omega_i = 1/\sigma^2$ (I).

The model, including anisotropic thermal motion for the Cs and Cr atoms and a secondary extinction correction,[20,21] refines to give a crystallographic R value of 5.8%. The resulting parameters are given in Table IV. The validity of the model is supported by the reasonable values of the thermal parameters on all atoms as well as the average Cr-C distance of 2.053(5) Å and average C-N distance of 1.14(1) Å which are in excellent agreement with the values obtained for the high temperature ($Fm3m$) refinement published previously.

As an additional test of the validity of the model, a final series of refinements were carried out using the parameters shown in Table IV as a starting model. In these refinements all constraints on the structural and thermal parameters were removed and the carbon and nitrogen thermal parameters were allowed to refine anisotropically. Although the R value for this refinement is significantly improved (3.6%), the resulting structure (Table V) differs from the constrained model only in insignificant detail, the improvement in fitting the x-ray intensities being due primarily to anisotropic motion of the $Cr(CN)_6$ octahedron.

*Work performed under the auspices of the U. S. Energy Research and Development Administration.

[1]W. Cochran, Phys. Rev. Lett. 3, 521 (1959).
[2]W. Cochran, Adv. Phys. 9, 387 (1960).
[3]W. Cochran, Adv. Phys. 10, 401 (1961).
[4]J. M. Worlock, in *Structural Phase Transitions and Soft Modes*, edited by E. J. Samuelsen, E. Andersen, and J. Feder (Universitetsforlaget, Oslo, 1972).
[5]J. F. Scott, Rev. Mod. Phys. 46, 83 (1974).
[6]B. I. Swanson and R. R. Ryan, Inorg. Chem. 12, 283 (1973).
[7]R. R. Ryan and B. I. Swanson, Inorg. Chem. 13, 1681 (1974).
[8]B. I. Swanson and L. H. Jones, J. Chem. Phys. 55, 4174 (1971).
[9]B. I. Swanson and L. H. Jones, Inorg. Chem. 13, 313 (1974).
[10]L. H. Jones, B. I. Swanson, and G. J. Kubas, J. Chem. Phys. 61 4650 (1974).
[11]E. Fukushima (unpublished).
[12]L. D. Landau, Phys. Z. Sowjetunion 11, 26 (1937).
[13]G. Ya. Lyubarskü, *The Application of Group Theory in Physics* (Pergamon, New York, 1960).
[14]J. L. Burman, Phys. Rev. Lett. 17, 1216 (1966).
[15]B. I. Swanson (unpublished).
[16]J. F. Scott and J. P. Remeika, Phys. Rev. B 1, 4182 (1970).
[17]J. L. Warren and T. G. Worlton, Comput. Phys. Commun. 8, 71 (1974).
[18]T. G. Worlton and J. L. Warren, Comput. Phys. Commun. 3, 88 (1972).
[19]C. E. Strouse, Acta Crystallogr. Sect. A 26, 604 (1970).
[20]W. H. Zachariasen, Acta Crystallogr. 23, 558 (1967).
[21]A. C. Larson, Acta Crystallogr. 23, 664 (1967).